APEM journal

Advances in Production Engineering & Management
Volume 18 | Number 3 | September 2023 | pp 288–302
https://doi.org/10.14743/apem2023.3.473

ISSN 1854-6250
Journal home: apem-journal.org
Original scientific paper

A feed direction cutting force prediction model and analysis for ceramic matrix composites C/SiC based on rotary ultrasonic profile milling

Amin, M.[a], Rathore, M.F.[b], Ahmed, A.A.[c], Saleem, W.[d,*], Li, Q.[e], Israr, A.[a]

[a]Institute of Space Technology, Islamabad, Pakistan
[b]University of Jeddah, College of Engineering, Department of Mechanical and Materials Engineering, Jeddah, Saudi Arabia
[c]University of Jeddah, College of Engineering, Department of Industrial and Systems Engineering, Jeddah, Saudi Arabia
[d]Technological University Dublin, Dublin, Ireland
[e]School of Mechanical Engineering & Automation, Beihang University, Beijing, P.R. China

ABSTRACT

Ceramic matrix composites have immense applications in the aerospace, aircraft, and automobile industries. Belonging to this class, carbon-fiber reinforced ceramic matrix composites (C/SiC) are used for critical applications due to their superior properties. However, these materials have also stringent properties of heterogeneity, anisotropy, and varying thermal properties that affect machining quality and process efficiency. So, developing a cutting force prediction model and analyzing machining parameters is an essential need for the accurate machining of such materials. In this study, a mechanistic-based feed direction cutting force prediction model for rotary ultrasonic profile milling of C/SiC composites is developed and validated experimentally. The experimental and simulation results closely match each other. The mean error and standard deviation were recorded as 1.358 % and 6.003, respectively. The parametric sensitivity analysis showed that cutting force decreased with increased cutting speed, whereas it increased with increased feed rate and cutting depth. The proposed cutting force model for rotary ultrasonic profile milling of C/SiC composites is robust and can be applied to predict cutting forces and optimize the machining process parameters at the industry level.

ARTICLE INFO

Keywords:
Rotary ultrasonic profile milling;
Modeling;
Ceramic matrix composites C/SiC;
Brittle fracture;
Cutting force;
Machining process optimization

**Corresponding author:*
waqas.saleem@tudublin.ie
(Saleem, W.)

Article history:
Received 27 October 2023
Revised 5 November 2023
Accepted 7 November 2023

1. Introduction

Ceramic matrix composites have gained growing attention in aerospace, automobile, and high-tech industries. Carbon fiber-reinforced ceramic matrix composites (C/SiC) exhibit attractive properties, which makes them an ideal candidate for diverse applications. For example, C/SiCs have a stable coefficient of friction, excellent wear resistance, high-run-in performance, and exceptional thermal stability at high temperatures [1, 2]. The typical usage of such materials includes developing brake discs (used in F16 Fighter, Porsche GT2, and French TGV NG) and manufacture of critical structural parts (e.g., nose cone, guide vane, and wings) for new generation aerospace vehicles and hyper-sonic vehicles [3]. These materials are also applied for developing nose cones and nozzles of rocket engines due to their better temperature resistance and lightweight

properties [4, 5]. However, due to high brittleness, anisotropy, and heterogeneity, the desired quality and efficiency of machined parts of such materials are challenging issues. High mechanical/ thermal loads and severe/ rapid tool wear were investigated [6]. So, machining difficult-to-cut materials with desired quality/ process efficiency was rigorous [7]. For efficient machining, cutting forces must be controlled within acceptable technical limits, as cutting force is the main index of the machining process [8, 9]. Due to excessive cutting forces, machining-induced defects, geometric/dimensional errors, and rapidly wear-off cutting tools were investigated [10]. Even though these materials developed near-to-net shapes, some machining processes are necessarily required to achieve final dimensions and surfaces [11]. With conventional machining processes like turning, drilling, milling, and grinding, issues related to quality and machining-induced defects are found in the machining of composite materials. Later, machining was found to improve with the invention of non-traditional machining processes such as electric discharge machining [38], ultrasonic machining, water jet machining, ultrasonic machining [39], vibration-assisted machining, rotary ultrasonic machining [31], electrolytic machining, chemical machining [12-14]. These machining technologies have shown better results for Ceramic matrix composites (CMC), Metal matrix composites (MMC), and Polymer matrix composites (PMC).

Rotary ultrasonic machining (RUM) was applied to drill glass material in 1966 [15]. Pei *et al*. [16] investigated rotary ultrasonic machining for milling of ceramics investigated. The hybrid machining process combines the material removal mechanism of diamond grinding process and ultrasonic machining. During this, a diamond abrasive core tool is ultrasonically vibrated in a normal direction with simultaneous spindle rotations. Prabhakar, 1992 worked on abrasive grit travels along its sinusoidal trajectory, causing hammering, abrasion, and extracting of workpiece material. The material removal occurs due to brittle fracture and the material flow plastically [16]. RUM is considered a rotary ultrasonic milling process if the abrasive core tool's feed direction is perpendicular to ultrasonic vibration's direction. However, when ultrasonic vibrations are applied in parallel to feed direction of abrasive core tool, the process is categorized as rotary ultrasonic drilling.

The published studies have shown that RUM demonstrates better machining for hard and brittle composite and ceramics. The cutting force is significantly reduced with RUM for ceramic matrix composites [16-18]. The improved surface integrity was investigated at the hole exit surface due to alteration of fiber fracture mechanism in rotary ultrasonic drilling of C/SiC composites [19]. Wang *et al*. [20] investigated that reduction in tearing size occurred by 30 % at hole exit with compound drill in rotary ultrasonic drilling of ceramic composite materials. The increase in ductile percentage was also investigated with increased spindle speed, while it decreased with increased vibration amplitude [21]. Hocheng *at al.* [22] analyzed improved machinability for rotary ultrasonic drilling of C/SiC composites. Li *at al.* [23] focused on advantages of RUM, considering cutting forces, material removal rate, and surface quality for CMC composites. Jiao *at al.* [24] studied the spindle speed and feed rate impact on cutting force. Bertsche *at al.* [25] found a significant decrease in cutting forces and tool wear for rotary ultrasonic slot milling of ceramic matrix composites. Ding *at al.* found a reduction in normal grinding force by 9-12 % and tangential grinding force by 9.7-19.4 %. The surface/sub-surface breakage decreased with ultrasonic grinding due to reduced grinding and ground surface roughness by 12 % compared to conventional grinding [26]. Yuan *at al.* [27] investigated the transition of ductile to brittle mode at a 4 μm depth of cut for rotary ultrasonic face milling of C/SiC composites.

In published literature, cutting force prediction models have been proposed to control cutting forces within acceptable limits. For instance, Yuan *at al.* [28] proposed a cutting force model for rotary ultrasonic face milling based on ductile mode for C/SiC composites. The cutting force models for rotary ultrasonic face milling of ceramics matrix composites (C/SiC) were established [29, 30]. Bertsche *at al.* [31] developed an analytical ultrasonic slot milling model of ceramic matrix composites.

The published studies have also reported the parametric sensitivity analysis and development of cutting force models for RUM of CMCs, like drilling, face, side, and slot milling. Other composite materials like glass (K9, BK7), PMC, and MMC have also been investigated for such machining pro-

cesses. However, rotary ultrasonic machining for profile/ contour milling has rarely been reported for composite materials. Profile milling is widely used in machining of composite materials. Keeping in view the challenges related to machining of C/SiC composites, there is an immense need for parametric investigation and development of a cutting force model for rotary ultrasonic profile milling of C/SiC composites to predict and control machining cutting forces to achieve better quality.

Novelty of the research

To the authors' knowledge, no study has been reported for rotary ultrasonic profile milling of composite materials for parametric analysis or cutting force model. The cutting force prediction model for rotary ultrasonic profile milling is reported in this research work. The presented research work is novel and provides new directions for machining composite materials.

This study develops a mechanistic-based model to predict feed direction cutting forces for rotary ultrasonic profile milling of Ceramic matrix composites-C/SiC. The model is developed by considering indentation fracture theory, brittle fracture, material removal mechanism, penetration trajectory, energy conservation theorem, and mathematical rules. The mathematical relationship of feed-cutting forces with parameters related to the machining process, workpiece material, and tool has been established. The cutting force prediction model is validated through data from experimental rotary ultrasonic profile milling of C/SiC composites.

The relationships between cutting force and machining parameters are investigated. This paper is organized into five sections. After the introduction, a mechanistic-based feed direction cutting force prediction model is developed in section 2. Section 3 explains experimental rotary ultrasonic profile milling for C/SiC composites. The results and discussion are covered in section 4. Finally, conclusions are presented in section 5.

2. Cutting force prediction model

This study applies rotary ultrasonic profile milling (RUPM) as the combination of ultrasonic vibration, grinding, and milling process, particularly with ultrasonic vibration perpendicular to the feed direction. During machining, the diamond abrasive core tool vibrates with ultrasonic frequency following a sinusoidal vibration path. The abrasive core tool's abrasive grits perform hammering, abrasion, and extraction (in sequence) in machining process. The material removal mechanism is based on indentation fracture theory. The rotary ultrasonic profile milling and trajectory of an abrasive grit are shown in Figs. 1(a), 1(b), respectively. The parameters and variables used in this study are given in Table 1. The following assumptions are made for the development of feed direction cutting force model: (a) diamond abrasive grits are rigid regular octahedron, (b) all diamond abrasive grits are of the same size, (c) material removal mode is a rigid brittle fracture.

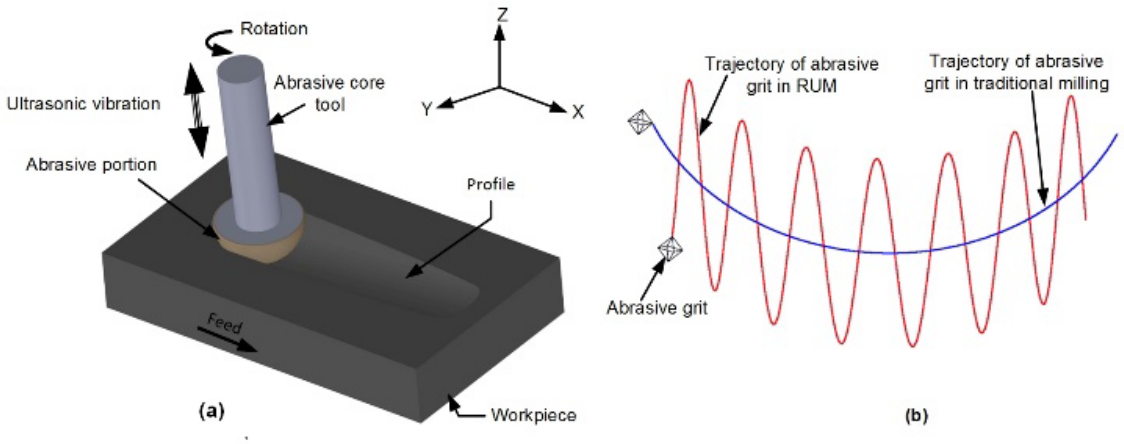

Fig. 1 Rotary ultrasonic profile milling process

Table 1 Parameters and variables applied in research work

Symbol/Abbreviation	Nomenclature
RUM	Rotary ultrasonic machining
RUPM	Rotary ultrasonic profile milling
CMC	Ceramic matrix composites
PMC	Polymer matrix composites
MMC	Metal matrix composites
MRR	Material removal rate of single abrasive grit, m^3/s
C/SiC	Carbon fiber-reinforced silicon matrix composites
β	Half angle of a diamond abrasive grit, 45°
S_a	The side length of a diamond abrasive grit, mm
w	Penetration depth of a diamond abrasive grit, mm
d	Penetration width of a diamond abrasive grit, mm
S	Spindle speed, rpm
a_p	Cutting depth, mm
f_r	Feed rate, mm/min
A	Ultrasonic vibration amplitude, 1×10^{-5} m
f	Ultrasonic vibration frequency, 20000 Hz
Z	Trajectory of a diamond abrasive grit, mm
Δt	Adequate contact time of penetration of grit in workpiece material, s
A_o	Area of the spherical abrasive core tool involved in cutting, mm
A	The radius of the spherical cap of the abrasive core tool, mm
h	Height of spherical cap of abrasive core tool, mm
R	The spherical radius of the abrasive core tool, mm
C_a	Abrasive concentration, mm
N_α	Number of active abrasive grits
C_l	Length of lateral crack, mm
C_h	Height of lateral crack, mm
d_c	Depth/ height of abrasive grit, mm
l_c	Abrasive grit length per vibration cycle, mm
l_{sec}	Chord length of segment/sector of abrasive grits (involved in cutting), mm
t	Adequate cutting time, s
K	Proportionality parameter for cutting force model
F_n	Cutting force of an abrasive grit on workpiece material, N
F_r	Radius cutting force by single grit, N
F_t	Tangential cutting force by single grit, N
F_f	Feed cutting force by single grit, N
$F_{f(m)}$	Cutting force measured from experiments, N
$F_{f(s)}$	Cutting force simulated from model without K, N
$F'_{f(s)}$	Cutting force simulated from model with K, N
V_r	Material removal volume by abrasive grit in one rotation cycle, m^3
V_r'	Material removal volume by a side face of active abrasive grit in one cycle, m^3
V_a	Actual material volume in one rotation cycle, m^3
θ	The angle between force F and cutting force F_n, (°)
v	Poisson's ratio
H_v	Vickers-hardness of the workpiece material, GPa
E	Elastic modulus, GPa
K_{IC}	Fracture toughness, $MPa\cdot m^{1/2}$
ρ	The density of workpiece material, g/cm^3
C_1, C_2, C_3	Dimensionless constants

2.1 Feed-cutting force model

The feed direction cutting force prediction model is developed by considering the single abrasive grit of the core tool. The summation of all active abrasive grits is considered in cutting process. When a diamond abrasive grit penetrates the surface of workpiece, the material undergoes plastic deformation. With increased penetration depth, median and lateral cracks grow, as shown in Fig. 2. The extended lateral cracks then induce and peel off the workpiece material. The median cracks are related to degradation of strength of workpiece material, while lateral cracks are involved in material removal in the machining process of composite materials. For developing the cutting force model, maximum penetration depth has used as an intermediate parameter to establish relationships between machining and related parameters with cutting force.

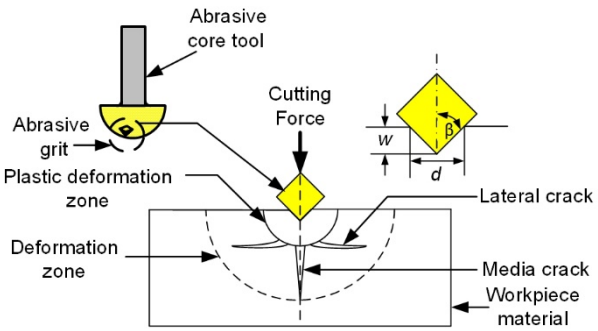

Fig. 2 Crack generation and deformation zone in material

From Fig. 2, the relationship can be established as follows:

$$w = \frac{d}{2\tan\beta} \tag{1}$$

where w is penetration depth, d is penetration width, and β is half-angle of abrasive grit ($\beta = 45°$). The volume of single diamond abrasive grit, v can be expressed as follows:

$$v = \frac{\sqrt{2}}{3} S_a^3 \tag{2}$$

where S_a is the side length of diamond abrasive grit, as shown in Fig. 3(a).

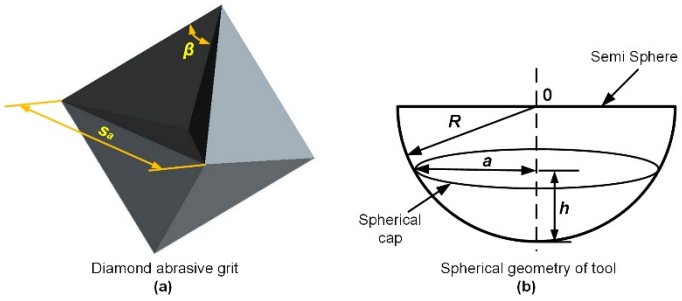

Fig. 3 Octahedron-shaped abrasive grit and related geometry

Diamond abrasive concentration in the working layer can be defined as the quantity of abrasives per unit volume. The concentration is the volume per cubic centimeter of abrasive grains containing 4.4 karats. An increase or decrease of 1.1 karats of the abrasives increases or decreases concentration by 25 %. According to this definition, the total number of active diamond abrasives/grits involved in cutting. N_α can be expressed as follows:

$$N_\alpha = \left(\frac{0.88 \times 10^{-3}}{(\sqrt{2}/3)\ S_a^3\ \rho}\ \frac{C_\alpha}{100}\right)^{2/3} A_0 = C_1 \frac{C_\alpha^{2/3}}{S_a^2} A_0 \tag{3}$$

where ρ is the density of diamond (3.52×10^{-3} g/mm^3), C_α is the diamond abrasive concentration, C_1 is a constant number, $C_1 = 3\times10^{-2}$ and A_0 is the area of abrasive tool in contact with the workpiece material (involved in cutting) at maximum cutting depth of the abrasive core tool. Since the spherical abrasive core tool is used in this study, the area of spherical cap of abrasive core tool is involved in cutting operation. The surface area of a closed spherical cap can be expressed as follows:

$$A_0 = \pi(a^2 + h^2) \tag{4}$$

where A_0 is the surface area of a closed spherical cap, a is the base radius circular sector, h is the height of the spherical cap, and R is the spherical radius of the abrasive core tool, as shown in Fig. 3(b). h shows the spherical sector's height from the base of spherical abrasive core tool. The radius of the circular sector is expressed as follows:

$$a = \sqrt{h\,(2R - h)} \tag{5}$$

From Eqs. 4 and 5, the effective surface area of the spherical core tool can be established as follows:

$$A_0 = 2\,\pi\,h\,R \tag{6}$$

Since the height of spherical cap of the tool is the height of spherical core tool involved in cutting process is the cutting depth a_p (i.e., $h \approx a_p$), the effective surface area of spherical core tool involved in machining can be expressed as follows:

$$A_0 = 2\,\pi\,a_p\,R \tag{7}$$

From Fig. 4, the relation between Z and f can be obtained as follows:

$$Z = A\sin(2\,\pi f t) \tag{8}$$

where Z represents the grain's trajectory, A and f are the magnitude and frequency, respectively, and t is the time.

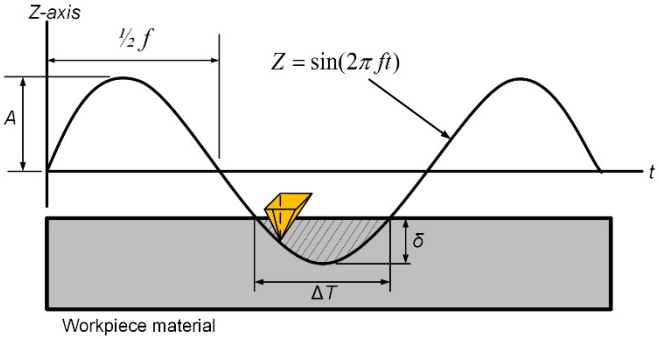

Fig. 4 Relation of adequate contact time (Δt) and maximum penetration depth (w)

During the machining, the cutting force in the feed direction is more than the axial direction; the feed direction cutting forces must be within acceptable limits. Developing a feed-cutting force model is essential for the prediction/ control of cutting forces for desired quality and reducing machining defects. The radial cutting force (F_r) and tangential force (F_t) for single diamond grit on the surface of abrasive core tool are shown in Fig. 5.

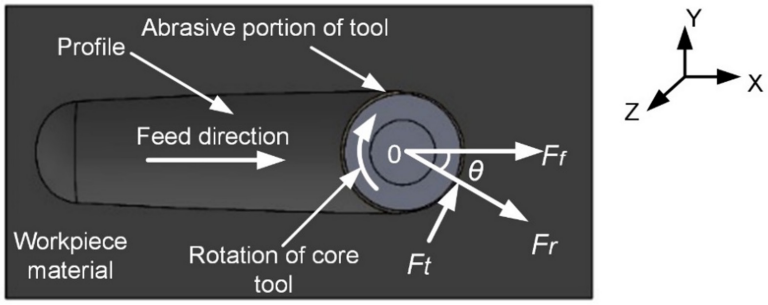

Fig. 5 Illustration of feed cutting force

The adequate cutting time in one rotation cycle is half of the cycle time, and can be expressed as follows:

$$t = \frac{1}{2}\,\frac{60}{S} = \frac{30}{S} \tag{9}$$

For cutting force in the feed direction, the active abrasive grits is expressed as follows:

$$N_\alpha = \left(\frac{0.88\,\times 10^{-3}}{(\sqrt{2}/3)\,S_a^3\,\rho}\,\frac{C_\alpha}{100}\right)^{2/3} l_c\,d_c \tag{10}$$

where l_c is the length of abrasive grit that travels in one vibration cycle, and d_c is the depth/height of abrasive grit (from the bottom of the spherical abrasive core tool).

Eq. 10 can be simplified by applying the factor $\left(\frac{0.88\times10^{-3}}{(\sqrt{2}/3)\,S_a^3\,\rho}\,\frac{C_\alpha}{100}\right)^{2/3}=\frac{C_1C_\alpha^{2/3}}{S_a^2}$

where $C_1=\left(\frac{0.88\times10^{-3}}{(\sqrt{2}/3)\,\rho}\,\frac{1}{100}\right)$

Eq. 10 can be expressed as follows:

$$N_\alpha=\frac{C_1C_\alpha^{2/3}}{S_a^2}l_c\;d_c \tag{11}$$

The factor $l_c\;d_c$ can be found by integrating (for side abrasive grits) from 0 to h for spherical abrasive core tool:

$$N_\alpha=\left(C_1\frac{C_\alpha^{2/3}}{S_a^2}\right)\frac{1}{2}\left(\int_0^h\sqrt{(2R-h)h}\;dh\right) \tag{12}$$

$$N_\alpha=\left(C_1\frac{C_\alpha^{2/3}}{S_a^2}\right)\frac{1}{2}\left(\frac{\pi\,R^2}{4}-\frac{1}{2}\left((R-h)\sqrt{R^2-(R-h)^2}+R^2\arctan\left(\frac{h}{\sqrt{R^2-(R-h)^2}}\right)\right)\right) \tag{13}$$

$$N_\alpha=\frac{1}{4}\left(C_1\frac{C_\alpha^{2/3}}{S_a^2}\right)\left(\frac{\pi\,R^2}{2}-\left((R-h)\sqrt{R^2-(R-h)^2}+R^2\arctan\left(\frac{h}{\sqrt{R^2-(R-h)^2}}\right)\right)\right) \tag{14}$$

$$l_{sec}=\frac{\pi\,R^2}{2}-\left((R-h)\sqrt{R^2-(R-h)^2}+R^2\arctan\left(\frac{h}{\sqrt{R^2-(R-h)^2}}\right)\right) \tag{15}$$

$$N_\alpha=\frac{1}{4}C_1\frac{C_\alpha^{2/3}}{S_a^2}l_{sec} \tag{16}$$

Also, the feed direction cutting force can be expressed as follows:

$$F_f=\int F_r\sin\theta\;d\;N_\alpha \tag{17}$$

where θ is the angle between the feed cutting and radial cutting forces.

$$F_f=2\int_0^{\frac{\pi}{2}}F_r\sin\theta\;d\;N_\alpha \tag{18}$$

By solving Eq. 18, the following relation can be obtained:

$$F_f=\frac{2\;F_r}{4}N_\alpha \tag{19}$$

where F_r is the radial cutting force by a single abrasive grit on the face of a spherical abrasive core tool, and F_n is the impact force exerted by a single abrasive grit ($F_r\approx F_n$). Eq. 19 can be expressed as follows:

$$F_f=\frac{F_n}{2}N_\alpha \tag{20}$$

The material volume removed by an abrasive grit in one rotation cycle, V_r can be found as follows:

$$V_r=2\;C_l\;C_h\;\pi\left[\int_0^h\sqrt{(2R-h)h}\,dh\right] \tag{21}$$

By considering the number of active abrasive grits on the spherical face, the material removal volume by spherical face of active abrasive grits in one rotation cycle V_r' can be expressed as follows:

$$V_r = 2\,C_l\,C_h\,\pi\left(\frac{\pi\,R^2}{4} - \frac{1}{2}\left((R-h)\sqrt{R^2-(R-h)^2} + R^2\arctan\left(\frac{h}{\sqrt{R^2-(R-h)^2}}\right)\right)\right) \tag{22}$$

The material removed by an abrasive grit in one rotation cycle is expressed as follows:

$$V_r = 2\,C_l\,C_h\,\pi\,\frac{1}{2}\,l_{sec} \tag{23}$$

$$V_r = \pi C_l\,C_h\,l_{sec} \tag{24}$$

The material removed by the side face of active abrasive grits in one rotation is given by:

$$V_r' = N_\alpha\,V_r \tag{25}$$

$$V_r' = N_\alpha\,\pi\,C_l\,C_h\,l_{sec} \tag{26}$$

The actual material removal in one rotation cycle is calculated by:

$$V_a = 2\,\pi\,R\,h\frac{60}{S}f_r \tag{27}$$

The relationship between V_r' and V_a is given by:

$$V_r{}' = K'\,V_a \tag{28}$$

where K' is a constant and can be found mechanistically from cutting force experiments. By putting values of $V_r{}'$ and V_a from Eq. 26 and Eq. 27, the following relation is obtained:

$$N_\alpha\,C_l\,C_h\,\pi\,l_{sec} = K'\frac{2\,\pi\,R\,h\,60\,f_r}{S} \tag{29}$$

According to the indentation theory proposed by Marshall and Lawn [32, 33], the lateral crack length C_l and the depth C_h can be expressed as follows:

$$C_1 = C_2\left(\frac{1}{\tan\beta}\right)^{5/12}\left(\frac{E^{3/4}}{H_v K_{IC}(1-v^2)^{1/2}}\right)^{1/2}F_n^{5/8} \tag{30}$$

$$C_h = C_2\left(\frac{1}{\tan\beta}\right)^{1/3}\frac{E^{1/2}}{H_v}F_n^{1/2} \tag{31}$$

where E is elastic modulus, ν is the Poisson's ratio of the workpiece material, and C_2 is a dimensionless constant number, $C_2 = 0.226$ [32, 33].

Using the values of C_l and C_h in Eq. 30 and replacing Eq. 31 with Eq. 29, the following relation is obtained:

$$F_n = (K')^{8/9}\frac{(120)^{8/9}\,R^{8/9}\,H_v^{4/3}\,(1-\nu^2)^{2/9}\,K_{IC}^{4/9}\,h^{8/9}\,f_r^{8/9}(\tan\beta)^{2/9}}{S^{8/9}\,C_2^{16/9}\,E^{7/9}\,l_{\sec}^{8/9}\,N_\alpha^{8/9}} \tag{32}$$

Putting the value of F_n from Eq. 32, Eq. 20 can be expressed as follows:

$$F_f = (K')^{8/9}\frac{(120)^{8/9}\,R^{8/9}\,H_v^{4/3}(1-\nu^2)^{2/9}\,K_{IC}^{4/9}\,h^{8/9}\,f_r^{8/9}\,(\tan\beta)^{2/9}\,N_\alpha^{1/9}}{2\,S^{8/9}\,C_2^{16/9}\,E^{7/9}\,l_{sec}^{8/9}} \tag{33}$$

By putting the value of N_α from Eq. 16, Eq. 33 can be expressed as follows:

$$F_f = (K')^{8/9}\,\frac{(120)^{8/9}\,R^{8/9}\,H_v^{4/3}(1-\nu^2)^{2/9}\,K_{IC}^{4/9}\,h^{8/9}\,f_r^{8/9}(\tan\beta)^{2/9}\,C_1^{1/9}\,C_\alpha^{2/27}l_{sec}}{2\,S^{8/9}\,C_2^{16/9}\,E^{7/9}\,l_{sec}^{8/9}\,S_a^{2/9}} \tag{34}$$

$$F_f = K\frac{C_3\,R^{8/9}\,H_v^{4/3}(1-\nu^2)^{2/9}\,K_{IC}^{4/9}\,h^{8/9}\,f_r^{8/9}(\tan\beta)^{2/9}\,C_\alpha^{2/27}}{S^{8/9}\,E^{7/9}\,l_{sec}^{7/9}\,S_a^{2/9}} \tag{35}$$

where C_3 is a constant and K is the proportionality parameter.

$$C_3 = \frac{(120)^{8/9}\, {C_1}^{1/9}}{2\, {C_2}^{16/9}} \qquad C_1 = 3{\times}10^{-2} \qquad C_2 = 0.226 \text{ [32, 33]}$$

Eq. 35 is the desired feed direction cutting force prediction model for rotary ultrasonic profile milling.

3. Experimental procedure

Experiments were conducted with different machining parameters to obtain the proportionality parameter K for validating feed direction cutting force model.

3.1 Experimental setup and conditions

The experimental rotary ultrasonic profile machining of C/SiC composite materials was conducted by using the experimental setup, as shown in Fig. 6. This setup comprises three parts, including the ultrasonic vibration system, CNC vertical machining center, and diamond abrasive spherical core tool. The ultrasonic vibration system contains an ultrasonic spindle and ultrasonic generator. The ultrasonic generator produces an ultrasonic frequency signal and provides to ultrasonic vibration spindle by producing ultrasonic vibrations with a specified amplitude. The ultrasonic vibration device containing an ultrasonic vibration spindle was fitted with a CNC vertical machining center (VMC 0850B, Shenyang, China). The cutting force was measured with a dynamometer (9257B, Kistler). The main specifications of the machine tool are given in Table 2. The mechanical properties of the workpiece material of C/SiC composites are in Table 3. The diamond abrasive spherical core tool parameters are mentioned in Table 4. The average grit size of 213 μm is calculated from supper abrasives (mesh size of 60/80 abrasive grits). The amplitude is kept on the higher side (10 μm), and ultrasonic frequency of 20000 Hz for optimum results (obtained through random experiments). The concave profile was selected for experimental machining with appropriate parameters. These are given in Table 5.

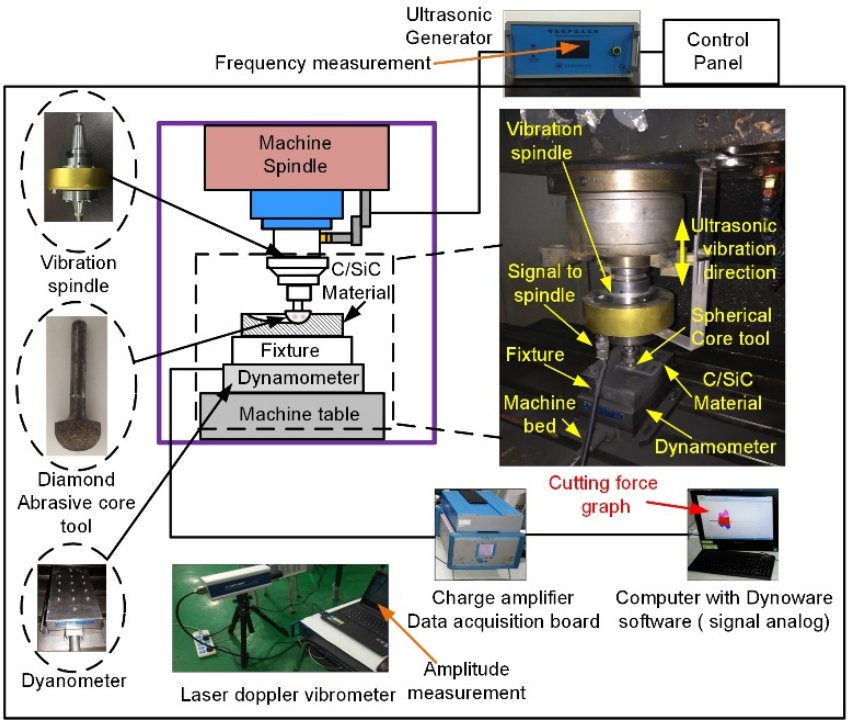

Fig. 6 Schematic along with actual setup for experiments

Table 2 Properties of the machine tool

Nomenclature	Specification
Spindle speed (with ultrasonic device)	0-6000 rpm
Ultrasonic amplitude (A)	10 μm
Ultrasonic frequency (f)	20000 Hz
Power consumption (Pw)	99 %

Table 3 Mechanical properties of C/SiC material

Nomenclature	Specification
Density (ρ)	2.0 g/cm^3
Porosity (P)	17-20 %
Tensile strength (σt)	≥ 40 MPa
Surface shear strength (σc)	≥ 10 MPa
Compression Strength(σy)	590 MPa
Elastic modulus (E)	67.7 GPa
Fracture toughness (K_{IC})	17.9 MPa·m$^{1/2}$
Vickers-hardness (H_v)	9.7GPa

Table 4 Properties of the abrasive core tool

Nomenclature	Specification
Tool type	Spherical
Abrasive	Diamond
Bond type	Metal-bond
Mesh size	60/80
Concentration (C_α)	100
Spherical radius (R)	8.25 mm

3.2 Experimental design

This study used important machining parameters, such as spindle speed, cutting depth, and feed rate based on various experimental observations for estimating effective cutting force. The experiments are designed in a single-factor experiment array with 3 factors. The level of each factor/parameter is selected by theoretical calculations, considering higher material removal rates and random experiments. The experimental design is given in Table 5.

Table 5 Experimental Design

Group	Experiments	Spindle speed S (rpm)	Feed rate f_r (mm/min)	Cutting depth a_p (mm)
1	1-7	1500, 2000, 2500, 3000, 3500, 4000,4500	100	1.0
2	7-12	3000	50,75, 100, 125, 150, 175	1.0
3	13-19	3000	60	0.7, 0.8, 0.9, 1.0, 1.1, 1.2

4. Experimental results and discussion

4.1 Measured cutting force

The experimental machining was conducted by selecting machining parameters corresponding to each group in the experimental design. The machining process is divided into three stages, i.e., enter, stable, and exit, corresponding to cutting force data (in graphical form), as shown in Fig. 7. Since profile machining is conducted in this study, the cutting force demonstrated peak values at maximum cutting depth. Therefore, the interval is considered for finding peak values of cutting force (as shown in Fig. 7). The cutting force value is the mean value of maximum values during the interval for peak value form obtained through graphical measurement with Dynoware software. The graphical cutting force data was transformed into numerical data through programming code developed in MATLAB software. The cutting force values obtained from experimental machining are shown in Table 6, corresponding to each group of parameters.

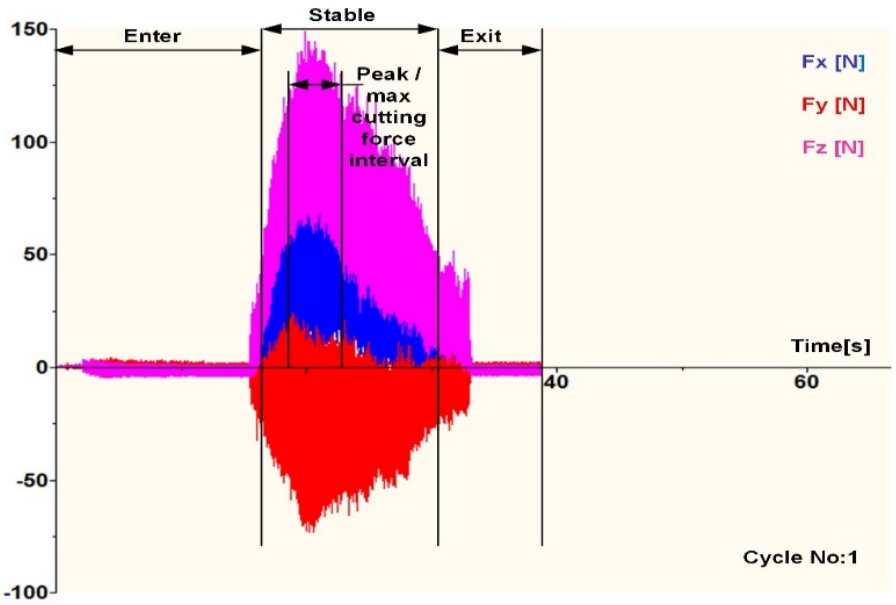

Fig. 7 Cutting force measurements (S = 2500 rpm, f_r = 100 mm/min, a_p = 1.0 mm)

4.2 The proportionality parameters

The simulated values of feed cutting force obtained through the cutting force prediction model are close to the measured cutting force when the factor gives the minimum value. The linear least square method was applied to find the value of K by partially differentiating the factor concerning K as follows:

$$\sum 2(F_{f(m)} - K\,F_{f(s)})(-F_{f(s)}) = 0 \tag{36}$$

By selecting the experimental and simulated feed cutting forces for each experiment group, the value of K was obtained as 34.842. This value gives the relationship between K and machining parameters. The simulated cutting force obtained with the feed cutting force model is given in Table 6.

Table 6 Measured and simulated feed force data

Exp. No.	S (rpm)	F_r (mm/min)	a_p (mm)	Measured feed force $F_{f(m)}$ (N)	Simulated feed force $F_{f(s)}$ without K (N)	Simulated feed force $F'_{f(s)}$ with K (N)	% Variation $\frac{F'_{f(s)} - F_{f(m)}}{F_{f(m)}}$ 100 %
1	1500	100	1.0	52.811	1.3498	53.998	+2.240
2	2000	100	1.0	50.720	1.3400	50.172	-1.080
3	2500	100	1.0	48.773	1.3324	46.423	-4.811
4	3000	100	1.0	45.615	1.3263	46.2109	+1.306
5	3500	100	1.0	42.165	1.3011	45.3329	+7.513
6	4000	100	1.0	38.508	1.2166	42.3887	+10.077
7	4500	100	1.0	43.140	1.3127	45.7370	+6.019
8	3000	50	1.0	36.426	1.1320	39.4411	+8.277
9	3000	75	1.0	45.263	1.2419	43.2702	-4.402
10	3000	100	1.0	47.263	1.3263	46.2109	-2.226
11	3000	125	1.0	48.816	1.3957	48.6289	-0.383
12	3000	150	1.0	52.763	1.4551	50.6985	-3.912
13	3000	175	1.0	59.763	1.5073	52.5173	-12.124
14	3000	100	0.7	41.127	1.3143	45.7928	+11.344
15	3000	100	0.8	42.323	1.3187	45.9461	+8.560
16	3000	100	0.9	45.754	1.3227	46.0855	+0.724
17	3000	100	1.0	46.023	1.3263	46.2109	-0.408
18	3000	100	1.1	46.599	1.3296	46.3259	-0.586
19	3000	100	1.2	50.431	1.4426	50.2630	-0.333

4.3 Analysis of measured and simulated cutting forces

The feed direction cutting forces obtained through experiments and simulated from the cutting force model are shown in Fig. 8. From the graph, simulated values of cutting forces closely match with measured cutting forces in most model parameter groups. However, higher variations are found only in three experimental groups (Exp. No. 6, 13, and 14).

The measured and simulated feed-cutting forces corroborate with experimental parameters. However, some higher variations (more than 10 %) are found for cutting forces in Exp. 6 (10.077 %), Exp. 13 (12.124 %), and Exp. 14 (11.344 %) (Table 6). The histogram error plots are shown in Fig. 9. The mean error is 1.358, with a standard deviation of 6.003. These variations predict the heterogenic and anisotropic properties of C/SiC composites. Also, considering the micro-perspective, SiC matrix is reinforced with a multilayer of carbon fibers, which causes uneven properties in feed and cutting depth directions. The proportion of SiC and carbon fibers differ in cutting area during RUPM, including the recorded variations between simulated and measured cutting forces. The generation of high temperatures causes cutting force variations.

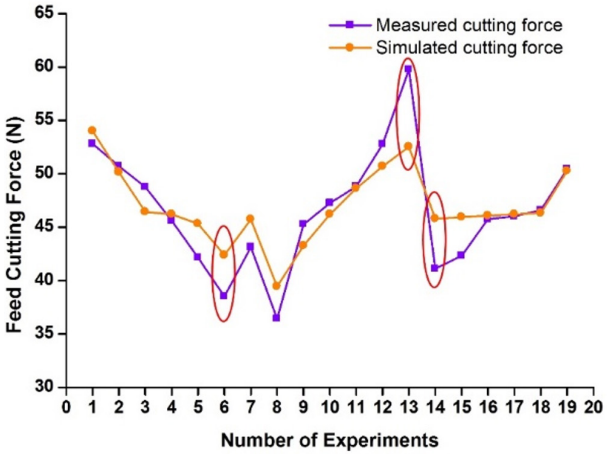

Fig. 8 Comparison of measured and simulated cutting force

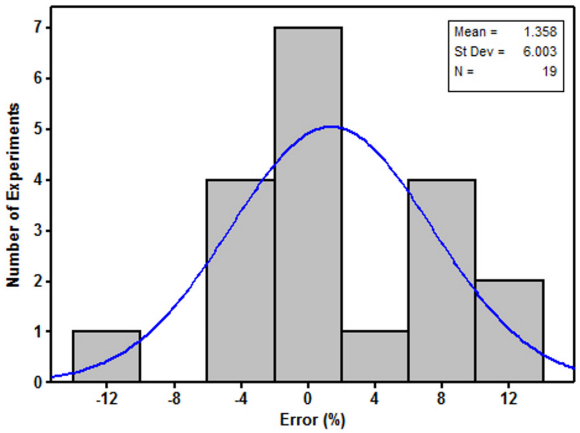

Fig. 9 Histogram plot of error vs. number of experiments

4.4 Comparison with published studies

Several studies have been reported on developing axial cutting force models for face, side, and slot milling of rotary ultrasonic machining of C/SiC composites. However, research work for the feed direction cutting force model has rarely been reported. Xiao *at al.* (2014) proposed a model for establishing cutting force during rotary ultrasonic slot milling of dental zirconia ceramics. They validated the cutting force model with max S = 6000 rpm, $f_r = 50$ mm/min, and $a_p = 0.19$ mm. However, the feed rate and cutting depth are significantly lower when considering material removal rates for practical applications. Li *at al.* [36] and Zhang *at al.* [37] proposed cutting force models for rotary ultrasonic face milling of C/SiC composites. The cutting force dynamic model has been proposed for rotary ultrasonic side milling of C/SiC composites.

4.5 Analysis of machining parameters

A feed rate of $f_r = 175$ mm/min and cutting depth of $a_p = 1.2$ mm is applied to develop a cutting force model. However, in published studies, such as Zhang *at al.* [29] and Xiao *at al.* [35] applied lower feed rate and cutting depth (f_r =12 mm/min, $a_p = 0.08$ mm, and $f_r = 50$ mm/min, $a_p = 0.190$ mm, respectively). This study used higher machining parameters to increase MRR and process efficiency for industrial applications. The feed-cutting forces found decreased with increased spindle speed. In contrast, the feed cutting forces found increased with the increase of feed rate and cutting depth. The relationship of feed cutting force with other machining parameters is shown in Fig. 10.

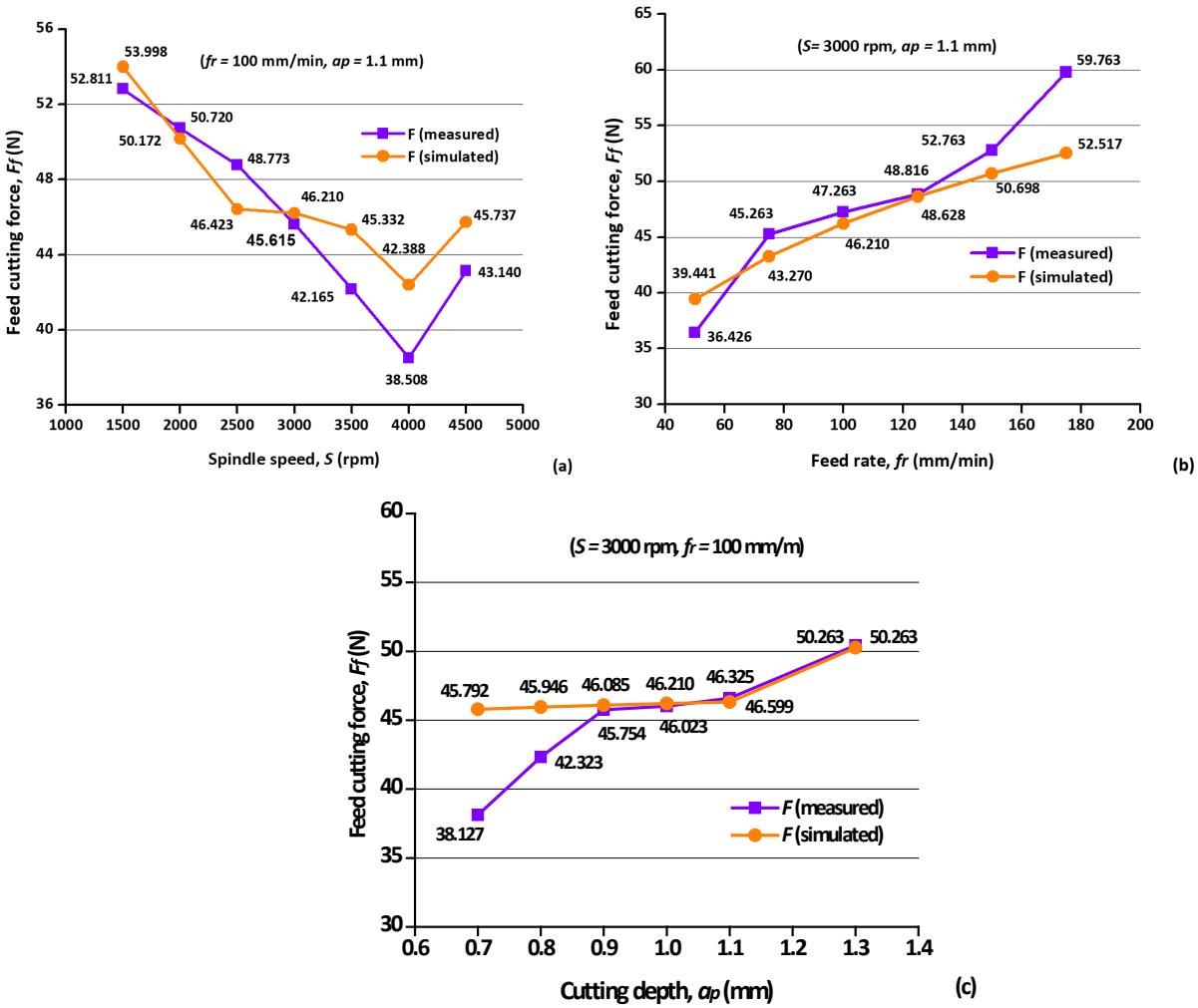

Fig. 10 Relationship of feed cutting force and machining parameters

5. Conclusion

In this study, rotary ultrasonic profile milling was conducted for machining C/SiC composites. The main contributions and conclusions of this research include:

- The cutting force prediction model is developed for RUPM of C/SiC composites and validated through experimental machining. The measured and simulated cutting forces closely match with each other. The mean error and standard deviation are 1.358 and 6.003, respectively. Variations of more than 10 % were recorded only for three groups of parameters due to material's heterogeneity and anisotropy. The developed feed cutting force prediction model is found robust and can be applied for prediction/control of cutting forces.
- The feed-cutting force prediction model for rotary ultrasonic profile milling of C/SiC composites is novel because no such study has been reported yet in published literature. This research work set new dimensions for the machining of composite materials.
- The higher machining parameters are applied ($f_r = 175$ mm/min, $a_p = 1.2$ mm, $S = 4500$ rpm) to achieve significantly higher material removal rates and practical machining conditions. The cutting force found decreased with the increase of spindle speed. However, the cutting force was increased with an increase in feed rate and cutting depth.
- The developed cutting force prediction model can be applied for predicting cutting forces in the feed direction, improving machined components' quality, and optimizing the machining process for rotary ultrasonic profile milling of C/SiC composites at the industry level.

Funding

This work was funded by the University of Jeddah, Jeddah, Saudi Arabia. The authors, therefore, acknowledge with thanks the University of Jeddah's technical and financial support.

Declaration of conflict of interest

The authors declare no conflict of interest.

References

[1] Chawla, K.K. (2003). *Ceramic matrix composites,* Second edition, Springer, New York USA, doi: 10.1007/978-1-4615-1029-1.
[2] Krenkel, W., Berndt, F. (2005). C/C–SiC composites for space applications and advanced friction systems, *Materials Science and Engineering: A,* Vol. 412, No. 1-2, 177-181, doi: 10.1016/j.msea.2005.08.204.
[3] Ferraiuolo, M., Scigliano, R., Riccio, A., Bottone, E., Rennella, M. (2019). Thermo-structural design of a ceramic matrix composite wing leading edge for a re-entry vehicle, *Composite Structures,* Vol. 207, 264-272, doi: 10.1016/j.compstruct.2018.09.024.
[4] Padture, N.P. (2016). Advanced structural ceramics in aerospace propulsion, *Nature Materials,* Vol. 15, 804-809, doi: 10.1038/nmat4687.
[5] Schmidt, S., Beyer, S., Knabe, H., Immich, H., Meistring, R., Gessler, A. (2004). Advanced ceramic matrix composite materials for current and future propulsion technology applications, *Acta Astronautica,* Vol. 55, No. 3-9, 409-420, doi: 10.1016/j.actaastro.2004.05.052.
[6] An, Q., Chen, J., Ming, W., Chen, M. (2021). Machining of SiC ceramic matrix composites: A review, *Chinese Journal of Aeronautics,* Vol. 34, No. 4, 540-567, doi: 10.1016/j.cja.2020.08.001.
[7] Teti, R. (2002). Machining of composite materials, *CIRP Annals,* Vol. 51, No. 2, 611-634, doi: 10.1016/S0007-8506(07)61703-X.
[8] Geng, D., Zhang, D., Li, Z., Liu, D. (2017). Feasibility study of ultrasonic elliptical vibration-assisted reaming of carbon fiber reinforced plastics/titanium alloy stack, *Ultrasonics,* Vol. 75, 80-90, doi: 10.1016/j.ultras.2016.11.011.
[9] Davim, J.P., Reis, P. (2005). Damage and dimensional precision on milling carbon fiber-reinforced plastics using design experiments, *Journal of Materials Processing Technology,* Vol 160, No. 2, 160-167, doi: 10.1016/j.jmatprotec.2004.06.003.
[10] Jawahir, I.S., Brinksmeier, E., , M'Saoubi, R., Aspinwall, D.K., Outeiro, J.C., Meyer, D., Umbrello, D., Jayal, A.D. (2011). Surface integrity in material removal processes: Recent advances, *CIRP Annals,* Vol. 60, No. 2, 603-626, doi: 10.1016/j.cirp.2011.05.002.
[11] Ding, K., Fu, Y., Su, H., Chen, Y., Yu, X., Ding, G. (2014), Experimental studies on drilling tool load and machining quality of C/SiC composites in rotary ultrasonic machining, *Journal of Materials Processing Technology,* Vol. 214, No. 12, 2900-2907, doi: 10.1016/j.jmatprotec.2014.06.015.
[12] Lau, W.S., Wang, M., Lee, W.B. (1990), Electric discharge machining of carbon fibre composite materials, *International Journal of Machine Tools and Manufacture,* Vol. 30, No. 2, 297-308, doi: 10.1016/0890-6955(90)90138-9.
[13] Kumar, J., Khamba, J.S. (2010). Modeling the material removal rate in ultrasonic machining of titanium using dimensional analysis, *International Journal of Advanced Manufacturing Technology,* Vol. 48, 103-119, doi: 10.1007/s00170-009-2287-1.
[14] Groover, M.P., (2010). *Fundamentals of modern manufacturing: Materials, processes, and systems,* Fourth edition, John Wiley & Sons, Hoboken, New Jersey, USA.
[15] Legge, P. (1966). Machining without abrasive slurry, *Ultrasonics,* Vol. 4, No. 3, 157-162, doi: 10.1016/0041-624X(66)90123-5.
[16] Pei, Z.J., Ferreira, P.M., Haselkorn, M. (1994). Rotary ultrasonic drilling and milling of ceramics, In: *Proceedings of the Design for Manufacturability and Manufacture of Ceramic Components Symposium, 96th Annual Meeting of the American Ceramic Society,* Indianapolis, USA, 1-12.
[17] Prabhakar, D. (1992). *Machining advanced ceramic materials using rotary ultrasonic machining process,* MS Thesis, University of Illinois Urbana-Champaign, Urbana, USA.
[18] Pei, Z.J., Ferrreira, P.M., Haselkorn, M. (1995). Plastic flow in rotary ultrasonic machining of ceramics, *Journal of Materials Processing Technology,* Vol. 48, No. 1-4, 771-777, doi: 10.1016/0924-0136(94)01720-L.
[19] Wang, J., Zhang, J., Feng, P. (2017). Effects of tool vibration on fiber fracture in rotary ultrasonic machining of C/SiC ceramic matrix composites, *Composites Part B: Engineering,* Vol. 129, 233-242, doi: 10.1016/j.compositesb.2017.07.081.
[20] Wang, J., Feng, P., Zheng, J., Zhang, J. (2016). Improving hole exit quality in rotary ultrasonic machining of ceramic matrix composites using a compound step-taper drill, *Ceramics International,* Vol. 42, No. 12, 13387-13394, doi: 10.1016/j.ceramint.2016.05.095.
[21] Pei, Z.J., Ferreira, P.M. (1999). An experimental investigation of rotary ultrasonic face milling, *International Journal of Machine Tools and Manufacture,* Vol. 39, No. 8, 1327-1344, doi: 10.1016/S0890-6955(98)00093-5.
[22] Hocheng, H., Tai, N.H., Liu., C.S. (2000). Assessment of ultrasonic drilling of C/SiC composite material, *Composites*

Part A: Applied Science and Manufacturing, Vol. 31, No. 2, 133-142, doi: 10.1016/S1359-835X(99)00065-2.
[23] Li, Z.C., Jiao, Y., Deines, T.W., Pei, Z.J., Treadwell, C. (2005). Rotary ultrasonic machining of ceramic matrix composites: Feasibility study and designed experiments, *International Journal of Machine Tools and Manufacture,* Vol. 45, No. 12-13, 1402-1411, doi: 10.1016/j.ijmachtools.2005.01.034.
[24] Li, Z.C., Jiao, Y., Deines, T.W., Pei, Z.J., Treadwell, C. (2005). Rotary ultrasonic machining of ceramic matrix composites: Feasibility study and designed experiments, *International Journal of Machine Tools and Manufacture,* Vol. 45, No. 12-13, 1402-1411, doi: 10.1016/j.ijmachtools.2005.01.034.
[25] Bertsche, E., Ehmann, K., Maluhin, K. (2013). Ultrasonic slot machining of a silicon carbide matrix composite, *International Journal of Advanced Manufacturing Technology,* Vol. 66, 1119-1134, doi: 10.1007/s00170-012-4394-7.
[26] Ding, K., Fu, Y., Su, H., Cui, F., Li, Q., Lei, W., Xu, H. (2017). Study on surface/ subsurface breakage in ultrasonic assisted grinding of C/SiC composites, *International Journal of Advanced Manufacturing Technology,* Vol. 91, 3095-3105, doi: 10.1007/s00170-017-0012-z.
[27] Yuan, S., Li, Z., Zhang, C., Guskov, A. (2018). Research into the transition of material removal mechanism for C/SiC in rotary ultrasonic face machining, *International Journal of Advanced Manufacturing Technology,* Vol. 95, 1751-1761, doi: 10.1007/s00170-017-1332-8.
[28] Yuan, S., Zhang, C., Hu, J. (2014). Effects of cutting parameters on ductile material removal mode percentage in rotary ultrasonic face machining, *Proceedings of the Institution of Mechanical Engineers, Part B: Journal of Engineering Manufacture,* Vol. 229, No. 9, 1547-1556, doi: 10.1177/0954405414548497.
[29] Zhang, C., Yuan, S., Amin, M., Fan, H., Liu, Q. (2015). Development of a cutting force prediction model based on brittle fracture for C/SiC in rotary ultrasonic facing milling, *International Journal of Advanced Manufacturing Technology,* Vol. 85, 573-583, doi: 10.1007/s00170-015-7894-4.
[30] Yuan, S., Fan, H., Amin, M., Guo, M. (2016). A cutting force prediction dynamic model for side milling of ceramics matrix composites C/SiC based on rotary ultrasonic machining, *International Journal of Advanced Manufacturing Technology,* Vol. 86, 37-48, doi: 10.1007/s00170-015-8099-6.
[31] Bertsche, E., Ehmann, K., Maluhin, K. (2013). An analytical model of rotary ultrasonic milling, *International Journal of Advanced Manufacturing Technology,* Vol. 65, 1705-1720, doi: 10.1007/s00170-012-4292-z.
[32] Marshall, D.B., Lawn, B.R., Evans, A.G. (1982). Elastic/plastic indentation damage in ceramics: The lateral crack system, *Journal of the American Ceramics Society*, Vol. 65, No. 11, 561-566, doi: 10.1111/j.1151-2916.1982.tb10782.x.
[33] Lawn, B.R., Evans, A.G., Marshall, D.B. (1980). Elastic/plastic indentation damage in ceramics: The median/radial crack system, *Journal of the American Ceramics Society,* Vol. 63, No. 9-10, 574-581, doi: 10.1111/j.1151-2916.1980.tb10768.
[34] Liu, D.F., Cong, W.L., Pei, Z.J., Tang, Y.J. (2012). A cutting force model for rotary ultrasonic machining of brittle materials, *International Journal of Machine Tools and Manufacture,* Vol. 52, No. 1, 77-84, doi: 10.1016/j.ijmachtools.2011.09.006.
[35] Xiao, X., Zheng, K., Liao, W. (2014). Theoretical model for cutting force in rotary ultrasonic milling of dental zirconia ceramics, *International Journal of Advanced Manufacturing Technology,* Vol. 75, 1263-1277, doi: 10.1007/s00170-014-6216-6.
[36] Li, Z., Yuan, S., Song, H., Batako, A.D.L. (2018). A cutting force model based on kinematics analysis for C/SiC in rotary ultrasonic face machining, *International Journal of Advanced Manufacturing Technology,* Vol. 97, 1223-1239, doi: 10.1007/s00170-018-1995-9.
[37] Zhang, C., Zhang, J., Feng, P. (2013). Mathematical model for cutting force in rotary ultrasonic face milling of brittle materials, *International Journal of Advanced Manufacturing Technology,* Vol. 69, 161-170, doi: 10.1007/s00170-013-5004-z.
[38] Tahir, W., Jahanzaib, M., Raza, A. (2019). Effect of process parameters on cutting speed of wire EDM process in machining HSLA steel with cryogenic treated brass wire, *Advances in Production Engineering & Management,* Vol. 14, No.2, 143-152, doi: 10.14743/apem2019.2.317.
[39] Liu, X., Wang, J., Zhu, J., Liew, P.J., Li, C., Huang, C. (2022). Ultrasonic abrasive polishing of additive manufactured parts: An experimental study on the effects of process parameters on polishing performance, *Advances in Production Engineering & Management,* Vol. 17, No. 2, 193-204, doi: 10.14743/apem2022.2.430.